



# Application of chemically-activated recycled carbon fibres for aqueous-phase adsorptions - part I: Optimisation of activation process

Jessica H. Taylor<sup>a</sup>, Gera Troisi<sup>b</sup>, Salman Masoudi Soltani<sup>a,\*</sup>

<sup>a</sup> Department of Chemical Engineering, Brunel University London, Uxbridge, UB8 3PH, UK

<sup>b</sup> Department of Mechanical & Aerospace Engineering - Institute for Health, Medicine & Environments, Brunel University London, Uxbridge, UB8 3PH, UK

## ARTICLE INFO

### Keywords:

Recycled carbon fibre  
Chemical activation  
Optimisation  
Design of experiment  
Adsorption

## ABSTRACT

Carbon fibre reinforced polymers (CFRPs) are an attractive and versatile material, owing to their low weight and high mechanical stability, among other characteristics. This has led to a rapid increase in their use across many industries, particularly the aviation and automotive sectors. However, large quantities of waste are being generated when CFRPs reach their end-of-life (EoL) due to limited recycling and reuse pathways. To create a circular economy for CFRPs, alternative, high-value EoL pathways for recycled carbon fibres (rCFs) are needed. At present, very few studies investigate the activation of rCFs, particularly for applications as adsorbents. Developing on from the authors' previous study, where rCFs were shown to be a promising precursor for the development of carbonaceous adsorbents, for applications in aqueous-phase, this work has focused on optimising the chemical activation procedure via a Box Behnken design-response surface methodology (BBD-RSM) approach, with an aim to maximise product yield and methylene blue adsorption capacity, using virgin carbon fibres (vCFs) as proof of concept. The optimum activated rCFs achieved an adsorption capacity of 454.55 mg/L; a significant increase of 715 % when compared to the previous study. While the optimum activated vCF counterpart achieved a maximum adsorption capacity 344.83 mg/L.

## List of abbreviations

ACF	Activated carbon fibre
ArCF	Activated recycled carbon fibre
AvCF	Activated virgin carbon fibre
BBD	Box Behnken design
CCD	Central composite design
CF	Carbon fibre
CFRP	Carbon fibre reinforced polymer
DoE	Design of Experiment
EoL	End of life
IR	Impregnation ratio
MB	Methylene blue
MB <sub>N</sub>	Methylene blue number
PAN-CF	Polyacrylonitrile-based carbon fibre
pH <sub>PZC</sub>	Point of zero charge
rCF	Recycled carbon fibre
RSM	Response surface methodology
S <sub>BET</sub>	Brunauer-Emmett-Teller surface area
vCF	Virgin carbon fibre

## 1. Introduction

Carbon fibre reinforced polymer (CFRP) use has expanded rapidly over recent decades, owing to their attractive properties such as high strength-to-weight ratio, and physical, chemical and fatigue resistance [1,2]. This has led to their application in a range of industries such as aviation, aerospace, automotive, wind energy and more (Fig. 1). The increasing popularity of CFRPs has culminated in a significant increase in carbon fibre (CF) production, which has seen a 180 % growth between 2006 and 2018; it has been predicted that the industry will continue to grow at a rate of up to 11 % per annum between now and 2030 [2,3]. PAN-based CFs are particularly popular within the aforementioned industries, owing to their excellent tensile strength, durability, low weight, chemical and thermal resistance [4–6].

However, the CFRP industry presents a major environmental challenge due to EoL products and off-cuts, with waste being projected to reach 20 kt annually by 2025 [2,8]. A publication in 2020, estimated that 35 % of EoL CFs were landfilled, 20 % recycled and only 2 % reused, within the UK [9]. The low recyclability and reuse for rCFs within their original applications are due to the compromised mechanical properties

\* Corresponding author.

E-mail address: [Salman.MasoudiSoltani@brunel.ac.uk](mailto:Salman.MasoudiSoltani@brunel.ac.uk) (S. Masoudi Soltani).

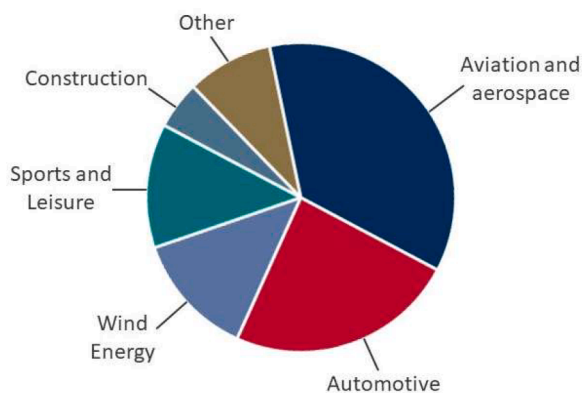


Fig. 1. Percentage of CFRP use within major industrial sectors.

following the recycling process resulting in a lack of trust around the use of rCFs in many industries. A factor contributing to the stigma around rCFs was the lack of legal standards to regulate the use of recycled materials within major industrial sectors [10]. Without a suitable market, recycling is not sustainable or profitable leading to waste going to landfill. However, landfill taxes increase annually driving the need for reduced waste generation and destinations for rCF materials. Therefore, to increase the sustainability of the CFRP industry, alternative rCF products with high-value applications must be identified.

In the last decade, researchers have sought to identify methods to improve the characteristics of rCF based CFRPs, such as introducing coatings such as nanoparticles and polymers to improve tensile and flexural strength, among other characteristics [11–15]. Alsaadi et al. investigated the introduction of silica nanoparticle coatings finding that the incorporation of 3 wt% silica resulted in an improvement in tensile strength by 20 % and flexural strength by 36 % [11]. Despite, many studies investigating the improvement of certain characteristics, there is little understanding around the degrading conditions (i.e. temperature, pH, moisture, exposure to seawater etc.) of rCF based products. In a review article produced by Isa et al. it was found that no degradation studies had been carried out on rCF-based CFRPs as of 2022, however it was hypothesised that degradation of rCF via the aforementioned pathways results in a reduction in mechanical strength, thermal stability and fatigue resistance [16]. Therefore, further research is required into the degradation conditions of rCF-based CFRPs before they can be widely reincorporated into the major industrial sectors, discussed previously.

At present there are several techniques to reclaim CFs from CFRP matrices each with their own advantages and disadvantages, the most common being mechanical, thermal (pyrolysis) or chemical (solvolysis) treatment. Pyrolysis is most widespread, owing to its industrially scalability, whilst leaving the valuable CFs intact. The process involves thermal decomposition of the epoxy resin by heating (450–700 °C) in an inert atmosphere (commonly N<sub>2</sub>). Under these conditions, the polymeric matrix is decomposed into lower-weight molecules and char, while the inert CFs remain largely unchanged, especially when the process is optimised for the feedstock that is being treated. The method can recover relatively long fibres retaining a high proportion ( $\leq 90$  %) of their mechanical properties [17,18]. However, a controlled post-treatment is required to remove any residual char without further degrading the fibres during combustion [19]. Furthermore, the method produces complex, hazardous mixtures in the chemical feedstock consisting of nitrogenous, oxygenated and sulphur-containing organic compounds mixed with water and off-gases such as carbon monoxide and dioxide, hydrogen, and low molecular weight hydrocarbons. Typically, the rCFs recovered using the above processes are used in low value applications such as fillers or low-performance reinforcements such as metal matrixes (e.g. aluminium alloy matrix composites) [16,20].

A review article on the recycling of CFs, published by Verma et al.

concluded that at present rCFs are not economically viable and in some cases may be more expensive to produce than vCFs, further highlighting the need for high-value applications for rCFs [21]. However, as of 2021, approximately 181 kt of CF were produced globally [8]. Assuming 10 % of annual CF production is scrap, waste or EoL material, this amounts to 18.1 kt tonnes of surplus waste. Studies have estimated that the average cost price of rCFs is approximately £9/kg [22,23]. By transitioning to recycling CFs over landfill or incineration, almost £163 million worth of rCFs could be introduced into the market. Additionally, further research into applications of rCFs could subsequently create value added products.

From an environmental perspective, the production rCFs have a much lower energy demand when compared to vCFs. It has been estimated that the reclamation of rCFs through pyrolysis processes produce around 5.4–11 kg/kg of CO<sub>2</sub> in comparison to PAN-based vCFs which are estimated to produce up to 31 kg/kg CO<sub>2</sub> [24–26]. While other disposal techniques such as incineration offer much lower CO<sub>2</sub> emissions of approximately 2.2–3 kg/kg, their energy demand is higher (32–34 MJ/kg) when compared to the pyrolysed rCF counterpart which has an energy demand of 2–30 MJ/kg and result in the destruction of a potentially high value product. [20,27].

Industrial-scale CFRP recycling has grown significantly with companies operating across Europe, USA and beyond. Gen2Carbon Ltd. (formerly ELG Carbon Fibre Ltd.) is a company based in the UK which specialises in recycling CFRPs on an industrial-scale, using pyrolysis processes. They have developed a continuous pyrolysis process capable of processing up to 5 t of waste per day. However, in general the rCFs produced are short in length and fluffy with lower mechanical strength, meaning they cannot replace vCFs in many sectors. Instead, rCFs are viewed as a new product that requires new processes and different designs. Previously, ELG had started a project aiming to establish a closed-loop recycling process for EoL aircraft CFRPs, they planned to achieve this by developing a new product using the rCFs [28].

Adsorbent production could be a promising industrial process for rCFs, since carbonaceous adsorbents are quickly gaining traction within many industries, owing to their high surface area, tuneable porosity, chemical stability, low cost and versatility [29–31]. Activated carbon fibres (ACFs) are a particularly attractive form of carbonaceous adsorbent due to their enhanced surface area to aspect ratio, high chemical resistance and tensile strength and low weight [32].

At present, very few articles investigate the conversion of rCFs to adsorbents via activation processes, particularly those recovered from CFRPs [4,33]. Despite the lack of research within this area, current studies are promising for production of ACFs from rCFs, due to the changes in structure during the recycling process. Research has reported that thermal treatment causes an increase in the interlayer spacing of the internal graphene layers, subsequently increasing the surface area prior to activation [34]. Furthermore, surface oxygen groups can be introduced during recycling processes which can act as active sites for adsorption. Some examples of oxygen-containing moieties on rCFs include carboxyl, hydroxyl and ketones [35]. Therefore, rCFs already possess pre-requisite chemical and physical properties that make them attractive candidates for applications as adsorbents in aqueous media. However, being a “new” adsorbent precursor, in depth research and process optimisation is paramount to enhance the characteristics of the material.

Statistical techniques such as design of experiment (DoE) are a useful optimisation tool to determine the impacts of various control variables on one or more response variables. Response surface methodologies (RSM) in particular enables the visualisation of relationships between control variables and their subsequent impact on the response variable [36]. Response surface techniques such as Box Behnken design (BBD) and central composite design (CCD) offer several advantages over traditional DoE techniques such as full factorial design or Taguchi. The key advantage being that RSM has the capability for response optimisation through a mixture of multiple regression and experimental

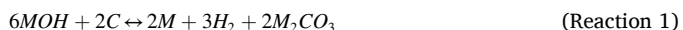
design, in addition to identifying significant parameters. Whereas, full factorial design and Taguchi only provide information on the later and therefore are often used for screening of adsorbents.

RSM is an invaluable statistical analysis tool when working with “new” precursor materials, allowing researchers to gain an insight into activation processes, by enabling the approximation of the relationship between a set of control variables/parameters ( $x_i$ ) and a given response ( $y$ ). This is achieved by establishing an empirical statistical model.

BBD is a particularly attractive optimisation technique in comparison to other response surface methodologies such as CCD, because it allows for the experimental process to be streamlined into the minimum number of experiments. Furthermore, the process avoids extreme experimental conditions which may result in loss of data (e.g. if all material is burnt off) or create a hazard for the operator. The effectiveness of an adsorbent is dependent on physiochemical characteristics such as surface area, pore size, surface functionality and etc. which in turn is dependent on the conditions applied during carbonisation and activation (e.g. temperature, hold time, impregnation ratio, flow rate etc.) and the subsequent application (e.g. aqueous or gaseous phase). For aqueous phase-applications, mesoporosity or hierarchical porosity is desirable, since larger pores aid the diffusion of pollutants into the internal porous network [32].

Activation techniques are traditionally divided into two sub-categories, namely, physical and chemical. The latter has a range of benefits including enhanced development of surface area and porosity at reduced temperatures and hold times, when compared to physical activation techniques [37–42]. Furthermore, carbonisation, activation and surface functionalisation can occur in tandem, significantly reducing processing steps [32]. However, the reagents can be costly, and the adsorbent requires an additional washing and drying steps after activation. KOH activation is an appealing technique for the development of aqueous-phase carbonaceous adsorbents, being able to create high surface areas with narrow pore size distribution, whilst being less costly than other chemical activation agents (e.g.  $H_2SO_4$  and  $H_3PO_4$ ). Furthermore, alkali metals such as potassium, possess the ability to intercalate between the graphene sheets of a carbonaceous structure, increasing the sheet-spacing and subsequently enhancing the specific surface area and pore volume [32,37,43,44].

It is generally accepted that the activation mechanism for hydroxides consist of overlapping redox reactions between the carbon surface and hydroxide, resulting in the expulsion of carbon from the adsorbent surface in the form of  $CO_2$  and  $CO$  (Reactions (1) and (2)) [42,45].



Dyes are widely applied within the textile industry, with an estimated 10,000 t consumed globally, per annum [46]. Methylene blue (MB) in particular, is one of the most prolifically applied dyes. MB is toxic, carcinogenic and non-biodegradable due to the stability of the aromatic ring structure (Fig. 2), creating environmental and human health concerns. It is also known to cause other harmful health effects such as high blood pressure, respiratory distress, mental disorders, anaemia, gastrointestinal pain, nausea and more [47–49]. Furthermore, its degradation products contain aromatic components which are potentially carcinogenic and mutagenic.

MB is highly water-soluble and enters the environment in large quantities through industrial discharges and effluents can be released into natural waterbodies in large quantities, creating an environmental concern. Furthermore, MB has an intense colour, and a high molar

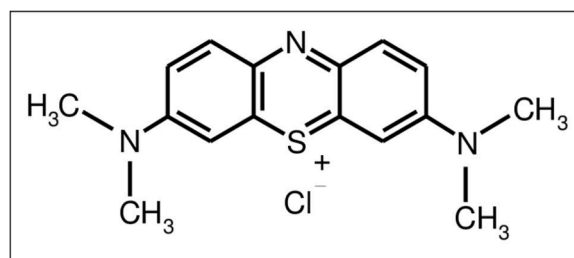


Fig. 2. Structure of methylene blue.

absorption coefficient ( $8.4 \times 10^4$  L/mol) even at low concentrations, which results in reduced sunlight transmittance within natural waterbodies [46]. Subsequently this causes a decrease in the photosynthetic ability of aquatic plants, and reduced chemical and biological oxygen demand, whereby anoxic conditions limit the aquatic biodiversity.

Building on from our previous study, where it was identified that rCFs are a suitable precursor for applications as adsorbents in aqueous media [33], in this paper, the authors have strived to optimise the physiochemical characteristics of the adsorbent by carefully employing design of experiment (DoE) techniques, specifically BBD, to investigate the activation process. This will be achieved by investigating the effects of several factors, namely, activation temperature, activation time and impregnation ratio (IR), to determine the impact on the pre-defined responses, yield and MB adsorption capacity. Additionally, in-depth characterisation will be undertaken pre- and post-activation, to study the impact of each treatment on the surface and physical and chemical characteristics of the activated rCF.

## 2. Materials and methods

### 2.1. Materials and reagents

The precursor rCFs in this study were G-TEX M, obtained from Gen2Carbon Ltd (West Midlands, UK), which was recovered from CFRPs using a modified pyrolysis process. All other chemical reagents were purchased from Fisher Scientific (UK).

### 2.2. Preparation of activated carbon fibre via experimental design

The preparation of ACFs consisted of combining rCFs with the defined quantity of KOH, as a wet mixture. The subsequent mixture was then placed into an aluminosilicate crucible, which was, in turn, positioned in the centre of an Inconel tube (Fig. 3). The furnace was supplied with  $N_2$  gas, at a flow rate of 100 ml/min. Whilst all other parameters (e.g. activation temperature, hold time and impregnation ratio) were determined by the BBD design, as discussed below (Table 1). Post-activation, the samples were retrieved from the tube and washed with 80 °C deionised water until a neutral pH was achieved, after which the fibres were dried overnight at 60 °C.

The authors opted to use an RSM methodology for the DoE, since the aim of the research was to optimise the activation procedure. BBD was selected as the experimental design method because it avoids the harshest conditions, preventing the complete burn-off of ACF. Furthermore, BBD is more economical, requiring a lower number of experimental runs when compared to CCD.

Experiments were set up to investigate the effects of three parameters (Table 1), namely, activation temperature ( $x_1$ , 670–830 °C), activation time ( $x_2$ , 0.5–3 h) and impregnation ratio (IR), ( $x_3$ , 1:1–1:10) on the response variables of yield ( $y_1$ , %) and adsorption capacity/methylene blue adsorption capacity ( $y_2$ ,  $q_e$ , mg/L), which were calculated using Eqs. (1) and (2), respectively.

$$\text{Yield } (y_1) = \frac{M_{\text{final}}}{M_{\text{initial}}} \times 100 \quad (1)$$

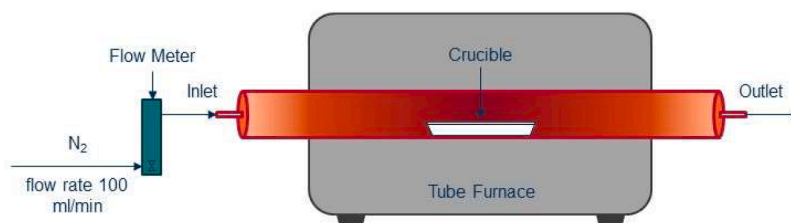


Fig. 3. Schematic of apparatus used during chemical activation.

Table 1

Parameters, codes and ranges of the BBD design.

Parameter	Code	Range
Activation Temperature (°C)	$x_1$	670–830
Hold Time (h)	$x_2$	0.5–3
IR (CF:KOH)	$x_3$	1:1–1:10

Where,  $M_{\text{initial}}$  and  $M_{\text{final}}$  are the mass of the CF before and after activation, respectively.

$$q_e(y_2) = \frac{(C_0 - C_e)V}{M} \quad (2)$$

Where,  $V$  is the volume of MB solution (L),  $M$  is the mass of adsorbent (g) and  $C_0$  and  $C_e$  are the initial concentrations (mg/L) and the equilibrium concentration of MB, respectively.

Upon the completion of the experimental campaign, the data set was analysed using ANOVA, to identify the statistically significant parameters and their combined effects. RSM was employed to optimise the activation process and visualise the interaction effects between factors, on a given response.

### 2.3. Sorbent characterisation

Properties of the precursors, activated and spent materials were investigated using Scanning Electron Microscopy/Energy Dispersive X-ray Spectroscopy (SEM/EDS, Supra 35VP), Fourier- Transform Infrared spectroscopy (FTIR, Perkin Elmer Spectrum One), and Raman spectroscopy (Renishaw Invia Raman Spectroscopy) with a 514 nm laser.

SEM was performed at a working distance of 4.5 and an accelerating voltage of 10 EkV, using a secondary electron detector for low magnification imaging. For high magnification imaging (>80,000) an intense detector was used at a working distance of 3.5 and accelerating voltage of 20 EkV. For EDS analysis the accelerating voltage was increased to 20 EkV and backscattered electron detectors were applied. Furthermore, copper tape was applied to prevent misinterpretation of the sample elements and the background.

FTIR was performed using the KBr method, due to the high absorbance of CFs. KBr was dried in an oven for a minimum of 48 h. Afterwards 1 mg of CF was combined with 300 mg of KBr and ground to a homogenous mixture using a pestle and mortar. The subsequent mixture was placed into a pellet-forming die and subjected to a force of 10 t for 5 min. The subsequent pellet was used for FTIR analysis in the region of 4000–500  $\text{cm}^{-1}$  for 20 scans at a resolution of 4  $\text{cm}^{-1}$ .

CHN elemental analysis was determined using a Flash 2000 Organic Elemental Analyser with an acetanilide standard. Proximate analysis was conducted via thermogravimetric analysis, according to ASTM D3172.

An SI analytics TitroLine 5000 automated titrator was used to perform the titrations for both the point of zero charge ( $\text{pH}_{\text{PZC}}$ ) and Boehm titrations. The mass titration technique was applied to determine the  $\text{pH}_{\text{PZC}}$  using established methods described by Noh and Schwarz [50]. Boehm titrations were conducted to determine the total acidity and basicity of the activated samples via a method described elsewhere

[51,52].

#### 2.3.1. Surface area determination

$\text{N}_2$  adsorption isotherms were employed using a Micromeritics ASAP 2020 sorption analyser to determine the surface area ( $S_{\text{BET}}$ ) and pore size distribution, by applying the Brunauer–Emmett–Teller (BET) and Barrett–Joyner–Halenda (BJH) methods, respectively. The analysis was carried out under  $\text{N}_2$  atmosphere at 77 K. Prior to this, the material was purged under  $\text{N}_2$  at 200 °C with a ramp rate of 5 °C/min, for 6 h.

Additionally, methylene blue number ( $\text{MB}_\text{N}$ ) was determined by investigating the adsorption properties of MB, which can be used as a tool to estimate the mesoporosity of CAs [53,54]. In summary,  $\text{MB}_\text{N}$  was determined by combining 0.005 g of ACF with varying concentrations of MB (25, 50, 100, 150, 200, 500 and 1000 mg/L). The subsequent mixtures were then shaken (200 rpm) for 24 h. Afterward, the ACFs were separated by decantation, and the remnant concentration of MB was measured using UV–Vis (Shimadzu UV Spectrophotometer), from which, the amount of MB adsorbed per gram of ACF was calculated using Eq. (2).  $\text{MB}_\text{N}$  was then determined using a linearised form of the Langmuir isotherm, (mg/g, Eq. (3)) [48,54].

$$\frac{c_e}{q_e} = \frac{1}{b q_{\text{max}}} + \frac{C_e}{q_{\text{max}}} \quad (3)$$

## 3. Results and discussion

### 3.1. Optimisation of chemical activation process

#### 3.1.1. Box Behnken design

In this work, a three-factor BBD was undertaken to determine the optimum conditions for the production of ACFs from rCF precursors

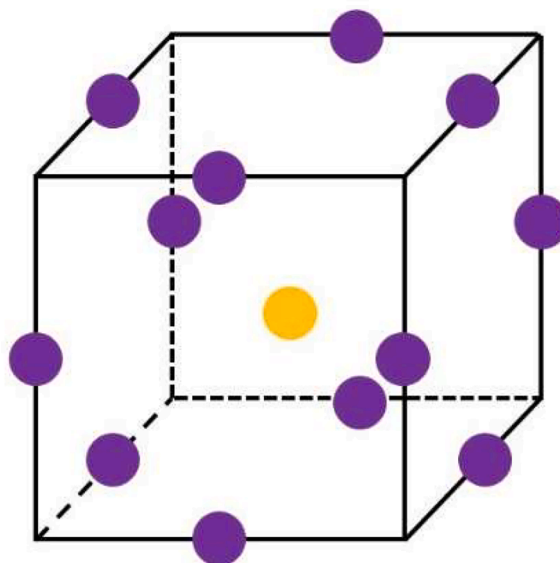


Fig. 4. Box–Behnken design space.

(Fig. 4).

The set of experimental conditions assayed are shown in Table 2. In order to interpret the results without the influence of systematic errors, the sequence for the experimental work was randomised. Data from experiments 1–12 were utilised to calculate the regression coefficients, whilst experiments 13–15 were replicates at the central point, used to assess experimental repeatability [55].

From the data, it can be observed that the highest yield of 104.80 was achieved during run 5. The increased yield was attributed to the intercalation of  $K^+$  ions, oxygen-containing moieties and the introduction of aluminosilicates due to corrosion of the combustion boat, as discussed further in Section 3.2. Furthermore, activation temperatures and times were set to their minimum levels of 670 and 0.5 h, respectively, whilst the IR was at the centre point of 1:5.5 (CF:KOH), meaning that there would be reduced carbon burn off, when compared to other experimental runs with harsher conditions.

ANOVA was applied as the statistical analysis technique to evaluate the model, determine the statistically significant factors and their subsequent impact on the responses, yield and MB adsorption capacity. The regression coefficient ( $R^2$ ) and predictive regression coefficient ( $R^2_{pred}$ ) of the model were calculated for both yield and adsorption capacity (Table 3). The latter value is of particular significance to determine the model's ability to predict the response for new observations. This is achieved by estimating the regression equation after the systematic removal of individual observations from a data set and therefore, determining the predictive capability of the model [45]. As can be seen in Table 3, both yield and adsorption capacity have high  $R^2$  values of > 95 %; however, a decrease is observed for  $R^2_{pred}$ , suggesting that the model may be inaccurate at predicting for new data points.

Table 4 shows the results for the ANOVA on the response yield. The  $p$ -value was applied to assess the significance of the factors and their interaction effects at a 95 % confidence level ( $p$ -value < 0.05). Both the non-linear and linear models were statistically significant with  $p$ -values of 0.004 and 0.001, respectively. Furthermore, the independent effects of all three factors, temperature, impregnation ratio and hold time were found to be statistically significant with  $p$ -values of 0.001, 0.001 and 0.030, respectively. From the data presented in Table 4, it is evident that a linear relationship exists within the design space due to the linear terms being most statistically significant.

The impacts of the three factors are shown clearly in the 3D contour plots (Fig. 5). When increasing parameters to their maximum value (+1), there is a distinct antagonistic effect on the yield, with activation temperature and impregnation ratio having the largest impacts. The large impact of activation temperature can be attributed to the enhanced

**Table 2**

BBD matrix with real and coded values of three factors studied, and responses yield and  $q_e$  of each run performed.

Run	Activation temperature (°C)		Activation time (h)		Impregnation ratio (CF:KOH)		Yield (%)		$q_e$ (mg/g)	
	$x_1$	Code	$x_2$	Code	$x_3$	Code	$y_1$	$y_2$		
	1	670	-1	1.75	0	1:1	-1	99.40	5.97	
2	830	+1	1.75	0	1:1	-1	52.35	6.07		
3	670	-1	1.75	0	1:10	+1	46.35	55.19		
4	830	+1	1.75	0	1:10	+1	3.79	58.74		
5	670	-1	0.5	-1	1:5.5	0	104.80	18.96		
6	830	+1	0.5	-1	1:5.5	0	58.18	11.49		
7	670	-1	3	+1	1:5.5	0	87.51	11.88		
8	830	+1	3	+1	1:5.5	0	24.65	7.86		
9	750	0	0.5	-1	1:1	-1	86.13	0.91		
10	750	0	0.5	-1	1:10	+1	38.19	49.40		
11	750	0	3	+1	1:1	-1	72.29	4.56		
12	750	0	3	+1	1:10	+1	23.43	55.13		
13	750	0	1.75	0	1:5.5	0	55.36	16.42		
14	750	0	1.75	0	1:5.5	0	69.30	45.22		
15	750	0	1.75	0	1:5.5	0	43.91	57.72		

**Table 3**

Regression coefficient and predicted regression coefficients for the responses in this study i.e. yield and adsorption capacity.

	$R^2$	$R^2_{pred}$
Yield	96.33	78.57
Adsorption capacity	99.03	84.41

**Table 4**

ANOVA results for the chemical activation campaign, when yield was investigated as the response.

Source (Yield)	F-value	P-value
Model	14.57	0.004
Linear	40.63	0.001
Temperature	56.63	0.001
Impregnation Ratio	56.25	0.001
Hold Time	9.01	0.030
Square	2.81	0.148
Temperature * Temperature	0.69	0.445
Impregnation Ratio * Impregnation Ratio	4.01	0.102
Hold Time * Hold Time	3.10	0.139
2-Way Interaction	0.27	0.844
Temperature * Impregnation Ratio	0.06	0.82
Temperature * Hold Time	0.75	0.425
Impregnation Ratio * Hold Time	0.00	0.963

etching of the carbon surface, which typically occurs at temperatures  $\geq 600$  °C, leading to the expulsion of carbon and tar, in the form of volatiles ( $CO_2$ , CO and  $H_2O$ ), developing the surface area and porous network, but subsequently decreasing the yield [32]. Furthermore, hydroxides such as KOH are known to enhance activation of CAs via overlapping redox reactions (Reactions (1) and (2)). Increasing the IR, results in a larger number of molecules available to etch the surface. Moreover, it has been hypothesised that the evolution of volatiles such as  $CO_2$ , CO and  $H_2O$  could further physically activate the CA, which would evolve in larger quantities at higher IR, further decreasing the product yield. Both steam and  $CO_2$  activation occur via dissociative chemisorption processes, where oxygen groups from water or steam molecules are exchanged with the surface, creating surface oxides, some of which are expelled as CO (Reactions (1) and (2)); in the case of  $CO_2$  this is known as the Boudouard reaction [32,56]. The expulsion of CO then enables the water gas shift reaction to occur (Reaction (8)), which is widely viewed as a key stage in physical activation processes.



$$y_1 = 649 - 1.2x_1 - 2.5IR + 3.6HT + 0.00063T^2 - 0.48IR^2 + 5.48HT^2 + 0.0031(T \times IR) - 0.041(T \times HT) - 0.041(IR \times HT) \quad (4)$$

Table 5 shows the ANOVA for the response MB equilibrium adsorption capacity. Similarly, to above, both the non-linear and linear models were statistically significant with  $p$ -values smaller than 0.05. In contrast to yield, only IR and the combined effects of IR squared were statistically significant with  $p$ -values of 0.000 and 0.001, respectively.

The contour plots for equilibrium adsorption capacity are shown in Fig. 6. Fig. 6A and C depict the dramatic impact of IR, with higher adsorption capacities being observed when IR is set to the maximum value. This can be attributed to the combined effects of several phenomena. Firstly, increased IR typically leads to enhanced development of porosity at due to elevated etching of the carbon surface, by the chemical activation agent. Furthermore, the intercalation of alkali metals such as  $K^+$  increases the spacing between graphene sheets, subsequently enhancing specific surface area and pore volume (Fig. 7).

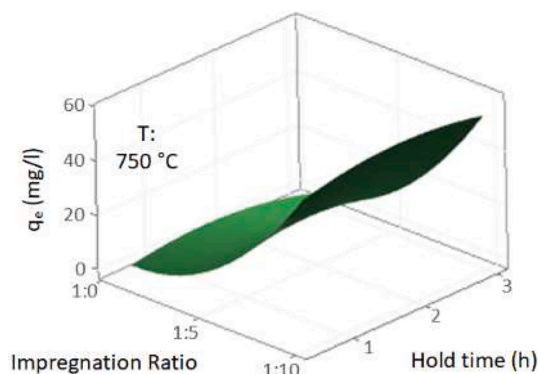
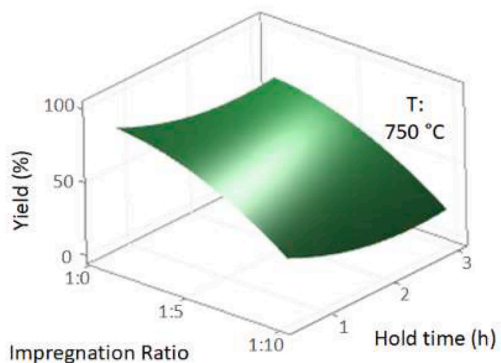
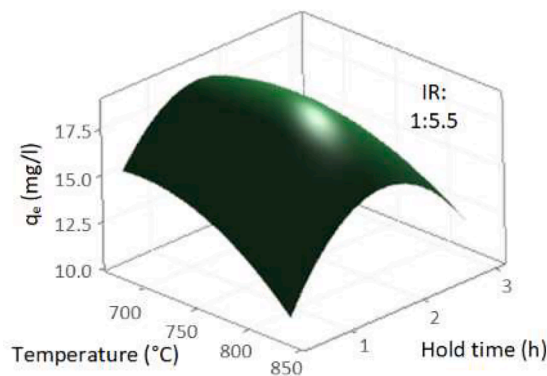
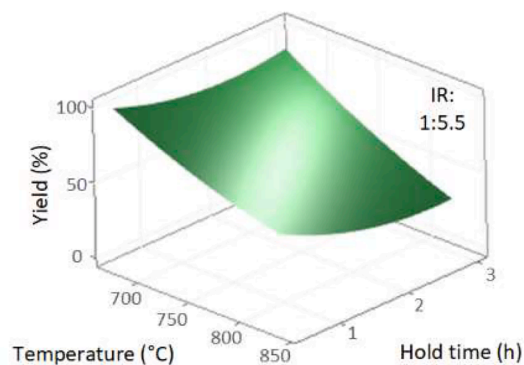
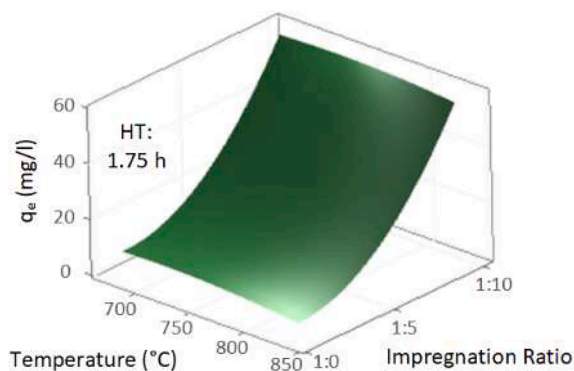
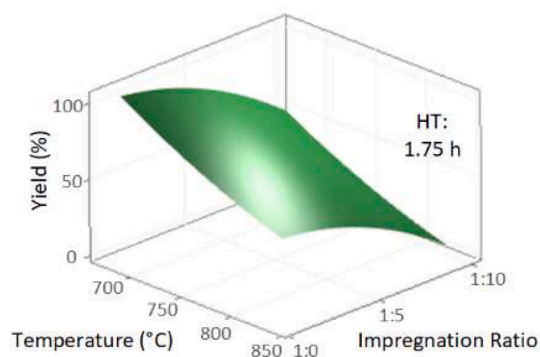


Fig. 5. 3D response surface plots for combined effects on the yield: (a) temperature and IR; (b) temperature and hold time; (c) IR and hold time.

Table 5

ANOVA results for the chemical activation campaign, when  $q_e$  was investigated as the response.

Source ( $Q_e$ )	F-value	P-value
Model	56.45	0.000
Linear	147.67	0.000
Temperature	1.14	0.335
Impregnation Ratio	441.71	0.000
Hold Time	0.16	0.704
Square	21.42	0.003
Temperature * Temperature	0.58	0.479
Impregnation Ratio * Impregnation Ratio	53.86	0.001
Hold Time * Hold Time	6.02	0.058
2-Way Interaction	0.25	0.857
Temperature * Impregnation Ratio	0.04	0.847
Temperature * Hold Time	0.25	0.636
Impregnation Ratio * Hold Time	0.46	0.527

Finally, a higher hydroxide ratio leads to an increased abundance of oxygen-containing moieties on the carbon-surface which act as active sites for adsorption.

Fig. 6. 3D response surface plots for combined effects on the MB adsorption value: (a) temperature and IR; (b) temperature and hold time; (c) IR and hold time.

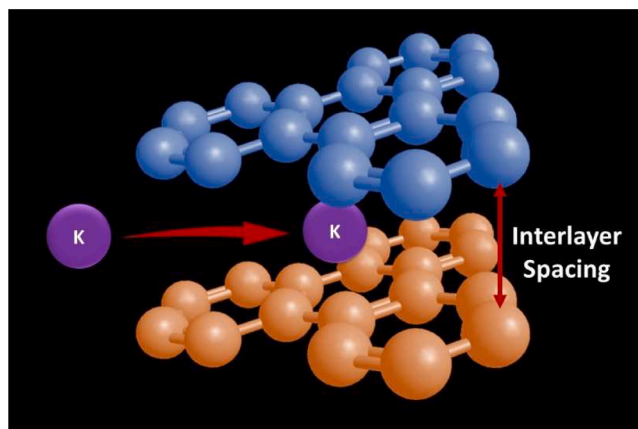


Fig. 7. Intercalation of  $K^+$  between graphene sheets.

$$y_2 = -92 + 0.28T - 2.5IR + 1.8HT - 0.00021T^2 + 0.65IR^2 - 0.28HT^2 + 0.00097(T \times IR) + 0.0086(T \times HT) + 0.21(IR * HT) \quad (5)$$

### 3.1.2. Optimum point validation and comparison with virgin carbon fibres

The model was validated via equally weighted dual-response optimisation, in order to optimise both yield and MB adsorption capacity. The optimum point was identified at an activation temperature of 670 °C, an IR of 1:10 and a hold time of 0.5 h. The resultant sample had a yield and adsorption capacity of 70.14 % and 19.04 mg/L, respectively. However, the response surface graphs depict that adsorption capacity could be further improved by increasing IR, whilst yield can be improved by reducing each factor beyond of the design space of this study. Therefore, a compromise was required when selecting optimum conditions to maximise both yield and adsorption capacity.

**3.1.2.1. Yield and impact of scale-up.** Fig. 8 depicts a parity plot, showing the actual experimental yield vs the predicted yield. From this, it can be concluded that Eq. (4) is a suitable model to predict and compare between experimental and model values, as shown by the reasonable  $R^2$  value of 0.89. It can be observed that there is a reduction in yield of the optimum point when compared to Runs 1, 5, 7, 9 and 11; however, this is to be expected due to the compromise made between yield and adsorption capacity, when selecting the optimum conditions.

The impact of scaling-up on the yield was also investigated for both ArCF-Opt and AvCF-Opt, by increasing the quantity of precursor by up to 8 times (Fig. 9). Despite some variation, scale up for AvCF-Opt has little to no effect on yield, maintaining yields greater than 70 % up to a precursor mass of 0.8 g. In contrast, scale-up did have an impact on the yield of ArCF-Opt, with a decrease of 27.7 % when scaling up from 0.1 g to 0.8 g of rCF. Despite the initial decrease in yield, the trend appears to plateau just above 40 % when the precursor mass is greater than 0.6 g, which is promising for industrial scalability. However, to truly determine industrial scalability, larger precursor masses should be investigated in future work.

**3.1.2.2. Methylene blue adsorption.** The parity plot for actual vs predicted adsorption capacity is shown in Fig. 10. A strong correlation is observed between the values, with an  $R^2$  value of 0.97 indicating that the model (Eq. (5)) can accurately predict experimental results.

The authors then developed on the previous study by assessing the  $MB_N$  of both the ArCF-Opt and AvCF-Opt.  $MB_N$  is a particularly useful

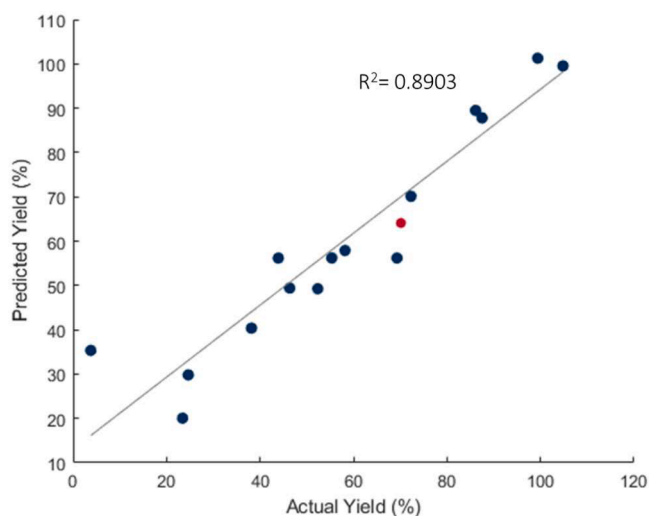


Fig. 8. Parity plot of the actual yield vs predicted yield, where (•) is the optimum point.

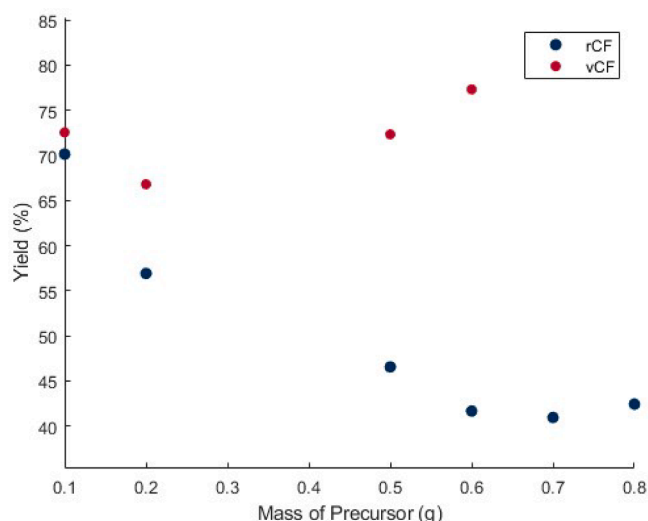


Fig. 9. Impact of scale up on yield.

tool to characterise the mesoporosity of aqueous-phase adsorbents, due to the molecule's molecular dimensions of 1.7, 0.76 and 0.33 nm (Fig. 11). Typically, adsorption is favoured when pore size is approximately 1.7 times larger than the second largest dimension of a molecule, meaning a large portion of MB would typically be adsorbed by mesopores, whilst a smaller portion may be adsorbed by micropores and macropores [32,53,57,58].

$MB_N$  is typically determined using a linearised form of the Langmuir isotherm (Eq. (3)) [54]. Using Eq. (3), the  $MB_N$  was calculated to be 454.55 and 344.83 for ArCF-Opt and AvCF-Opt, respectively. Considering the specific surface area of ArCF and AvCF were comparable (Table 6), it was concluded that the increased surface functionalisation of ArCF played a crucial role in MB adsorption due to the enhanced chemisorption.

## 3.2. Material characterisation

This section will discuss the physicochemical characteristics of the precursor and optimum ACF samples.

### 3.2.1. Surface analysis

**3.2.1.1. Physical surface analysis.** The BET surface area ( $S_{BET}$ ), pore volume and pore size were measured and calculated for both ArCF-Opt and AvCF-Opt (Table 7). The  $S_{BET}$  for both ACFs were comparable of  $> 400 \text{ m}^2/\text{g}$ . The slightly higher surface area for ArCF was attributed to the reduction in mechanical strength during the recycling process, meaning that the carbonaceous framework is more readily etched away by the activation agent and thus, increasing surface area. Furthermore, ArCF had a higher total pore volume, despite having a smaller micropore volume. This indicates that ArCF has a higher volume of meso and macropores, which typically aid internal diffusion of adsorbates in aqueous phase adsorption.

**3.2.1.2. Chemical surface analysis.** Boehm titrations were applied to determine the total acidity and basicity of the samples. The number of moles of acidic surface groups was determined using Eq. (6), whereas the basic surface groups were calculated using Eq. (7). The number of moles per gram of adsorbent was then determined using Eq. (8).

The total number of surface groups are presented in Table 8, it can be seen that ArCF-Opt samples possess significantly higher levels of all surface groups when compared to AvCF-Opt, particularly for carboxyl and basic groups. Typically, rCFs are short and fluffy in length, with some minor defects. Furthermore, thermal treatment during recycling

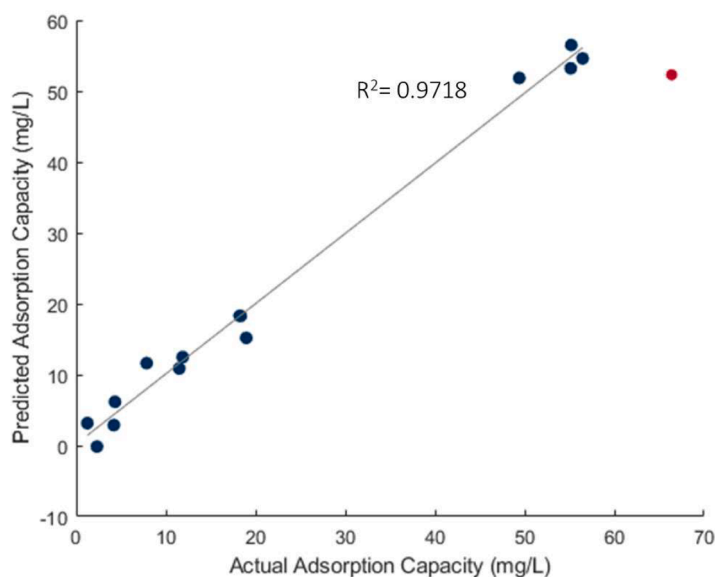


Fig. 10. Parity plot of the actual adsorption capacity vs predicted adsorption capacity, where (•) is the optimum point.

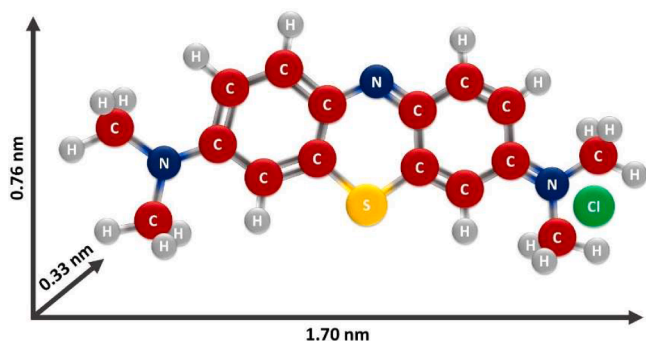


Fig. 11. Dimensions of MB.

Table 6  
Comparison of  $S_{BET}$  and  $q_{max}$  for ArCF, AvCF and other carbonaceous adsorbents.

Sample	$S_{BET}$	$q_{max}$	Ref
ArCF	428	454.55	This work
AvCF	415	344.83	This work
ACF	1975	729.00	[59]
ACF	1614	325.83	[60]
ACF	1801	478.50	[61]
AC	1172	162.54	[47]
AC	2132	333.30	[48]
AC	708	241.30	[62]
AC	594	180.00	[63]

Table 7  
Textural properties of ArCF and AvCF based on the BET  $N_2$  adsorption isotherm and MB adsorption.

Sample	$S_{BET}$	$V_{micro}$	$V_{total}$	Pore size	$MB_N$
ArCF	427.63	0.02	0.35	4.08	714.29
AvCF	414.88	0.04	0.33	4.20	400.00

has been shown to increase the interlayer distance between the internal layers of CFs creating a larger available surface area for oxidation (Fig. 12).

Furthermore, some oxidative effects have been reported during thermal recycling processes meaning that the rCF precursor may already

Table 8  
Chemical surface analysis of ArCF and AvCF based on Boehm titrations.

Sample	Quantity of surface groups mmol/g			
	Carboxyl	Phenol	Lactone	Basic
ArCF	2.41	0.29	0.31	2.32
AvCF	0.07	0.07	0.11	0.03

possess a number of oxygen-containing moieties prior to activation [34].

$$n_{CSF} = \frac{n_{HCl}}{n_B} [B]V_B - ([HCl]V_{HCl} - [NaOH]V_{NaOH}) \frac{V_B}{V_a} \quad (6)$$

$$n_{CSF} = [B]V_B - [HCl]V_{HCl} \frac{V_B}{V_a} \quad (7)$$

Where,  $n_{CSF}$  is the number of moles of surface functional groups and  $\frac{n_{HCl}}{n_B}$  is the molar ratio of HCl to reaction base. [B], [NaOH] and [HCl] are the concentrations of reaction base, NaOH and HCl, respectively.  $V_B$  and  $V_{HCl}$  are the volumes of reaction base and HCl, respectively.  $V_a$  is the volume of the aliquot taken from  $V_B$ .

$$\eta_{CSF} = \frac{n_{CSF}}{M_C} \quad (8)$$

$\eta_{CSF}$  is the number of moles of surface groups per g of adsorbent and  $M_C$  is the mass of carbon.

### 3.2.2. SEM-EDS

SEM images of the recycled and virgin carbon fibres, pre-activation, are presented in Fig. 13, whilst the activated samples are shown in Fig. 14. Fig. 13A and B depict the non-activated CFs at 20,000x magnification, displaying a smooth fibrous form with some striations on the surface. A similar image was depicted for the activated samples in Fig. 14A and B, with some visible surface defects.

Fig. 14C and D depict the ACFs at a magnification of 150,000x, revealing the external porous structure. A heterogenous surface consisting of meso- and macropores were observed for both recycled and virgin ACFs, with pore sizes ranging between 11.88 and 59.40 nm, in agreement with the  $S_{BET}$  data, which indicated a high meso- and macropore volume of  $> 0.31 \text{ cm}^3/\text{g}$ . Interestingly, the porous structure for the ArCFs appeared to be angular in shape, whereas the AvCF porous network appeared to be orbicular. The microporous structure was absent from the SEM imaging due to limited resolution, in order to image the

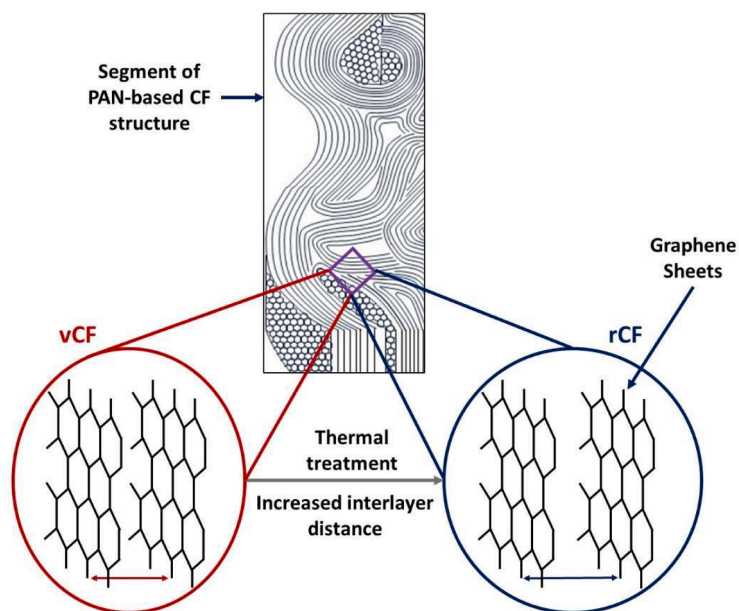


Fig. 12. Comparison between the interlayer distance of vCFs vs rCFs.

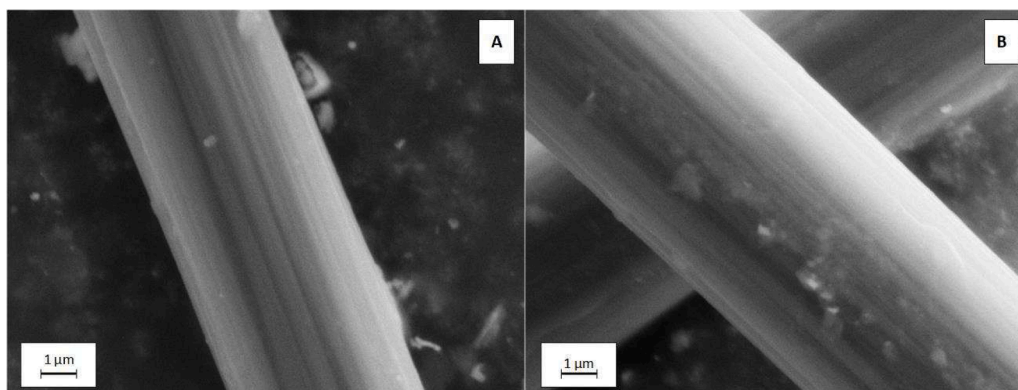


Fig. 13. SEM imaging of rCF (A), vCF (B) at 20,000x magnification.

microporous structure, alternative techniques such as TEM would need to be applied, however the applicability of this technique is highly dependent on the crystallinity of the material and would not be useful for highly amorphous samples.

The EDS results of the rCFs are shown in Fig. 15. In general, a high carbon content of up to 100 % was observed; however, realistically this would not be the case since EDS isn't a particularly sensitive technique. Additionally, some known elements within the CF structure, such as nitrogen and hydrogen could not inherently be identified during EDS. The former element isn't readily detected due to its low-Z number and its overlapping with the carbon and oxygen K-alpha. Whilst hydrogen atoms only possess a  $1s^1$  electron shell, and since core electrons can't be removed, x-ray emission is not possible. In some of the analysed areas, small amounts of oxygen and potassium were identified which was ascribed as impurities introduced during the CF recycling process.

Post-activation, there was a distinct drop in the carbon content of the ArCFs to < 72 %, which can be attributed to the expulsion of carbon in the form of VOCs during the activation process, combined with the introduction of oxygen containing moieties and potassium into the ACF structure, which in turn may have decreased the amount of carbon (in percentage terms). The increased K content was attributed to the intercalation of  $K^+$  ions between the graphene sheets of the carbonaceous structure; a well-known activation mechanism when applying

alkali activation agents [32]. This was also confirmed by the notable increase in the fibre diameter of the activated samples, with the average diameter of rCF and vCF increasing by 13.95 % and 0.67 %, respectively.

A number of crystalline impurities were identified on the surface after activation, which was due to corrosion of the aluminosilicate crucible by the KOH activation agent, leaving residue on the fibre surface. EDS analysis of the crystalline deposits identified the presence of small amounts of Al and Si of 1.51 % and 1.77 %, respectively (Fig. 15B). The EDS also identified some small amounts of copper, which was attributed to the use of copper adhesive tape during the SEM-EDS analysis and therefore, was excluded from the weight % calculations.

### 3.2.3. Elemental analysis

The elemental analysis of the rCF and vCF before and after activation are shown Table 9. Prior to activation, both rCF and vCF demonstrated a carbon content above 90 %, in accord with the IUPAC definition for carbon fibres. Additionally, both CFs have a nitrogen content greater than 3 %, which is typical of PAN-based CFs. Furthermore, rCFs possess an oxygen content of almost double that of vCFs which was attributed to oxidation during recycling processes.

In agreement with the EDS data, after activation, there is a notable reduction in carbon content to less than 80 % which can be attributed to the burn-off of fixed carbon and expulsion of volatile organic carbons

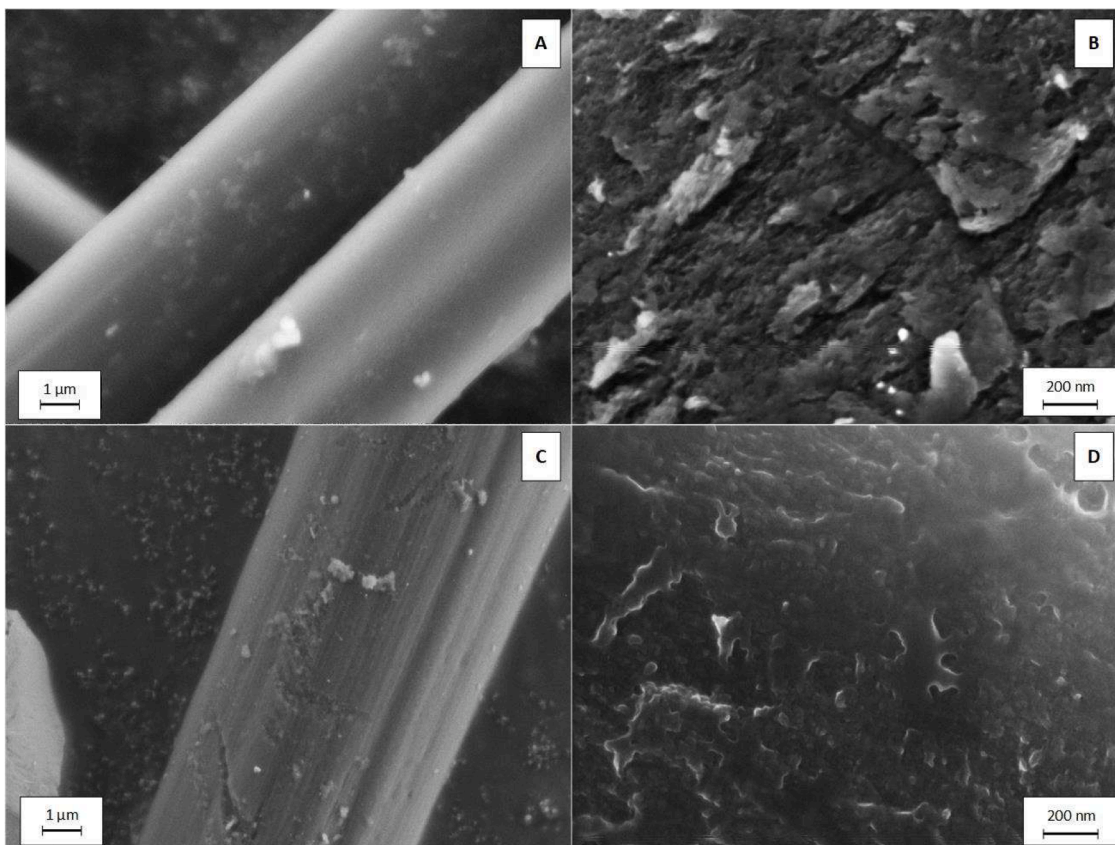


Fig. 14. SEM imaging of ArCF (A), AvCF (C) at 20,000x magnification and ArCF (B), AvCF (D) at 150,000x magnification.

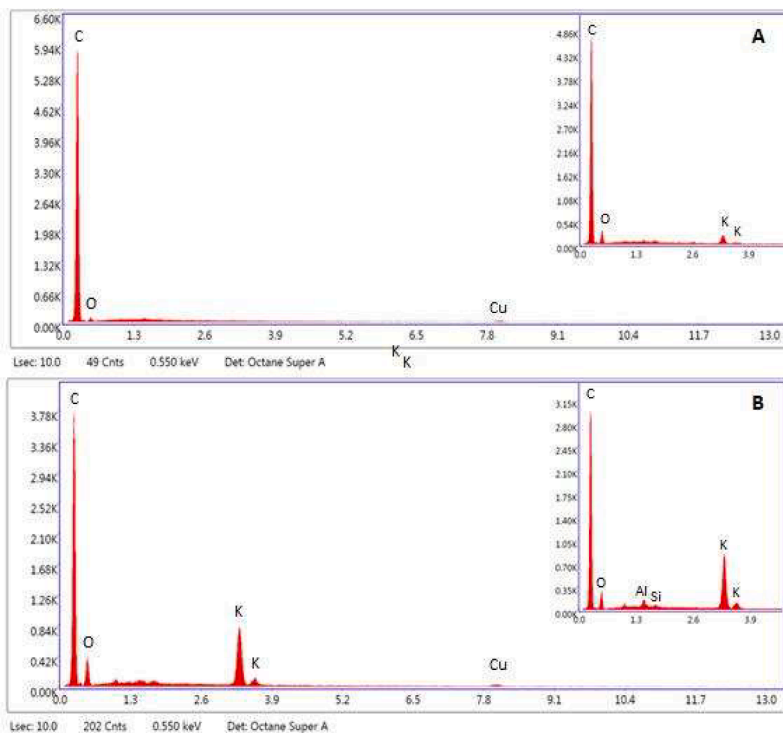


Fig. 15. EDS spectra of rCF (A) and ArCF (B).

(VOCs) during the activation process. Furthermore, the nitrogen content for both virgin and recycled ACFs has almost halved in comparison to their precursor counterparts, which can be attributed to the cleaving of

C–N bonds at elevated temperatures. As expected, there is a significant increase in oxygen content after the activation, due to the application of alkali activation agents which are well known to introduce oxygen-

**Table 9**  
Elemental analysis of precursor and activated carbon fibres.

Sample	C (%)	H (%)	N (%)	O (%)
rCF	93.87	0.28	4.07	1.78
vCF	95.32	0.43	3.32	0.93
ArCF-Opt	78.19	0.53	2.34	18.94
AvCF-Opt	78.20	0.53	1.88	19.39

containing groups into the carbonaceous framework via overlapping redox reactions (Reactions (1) and (2)). The groups introduced can be acidic or basic in nature and typically consist of lactone, carboxyl, phenol, lactol, pyrone, ketone and chromene groups (Fig. 16).

### 3.2.4. Proximate analysis

Proximate analysis was employed to quantify the amount of fixed carbon, volatile organic compounds (VOCs), water and ash (Table 10). This was achieved by firstly elevating the temperature under an inert atmosphere to determine the amount of VOCs and water, after which, the gas flow was switched to an oxidising atmosphere to eliminate fixed carbon, the residual mass signified the ash content.

After activation, a significant reduction in fixed carbon content was observed, in agreement with the EDS and CHN analysis. Furthermore, there is a significant increase in VOC, water and ash content post-activation. The large increase in VOC content post-activation is atypical for carbonaceous adsorbents. It is well-known that VOCs are emitted from the structure during activation; however, the observed increase in VOC% may have been inflated in terms of percentage, due to the significant decrease in carbon content (due to decomposition), and consequently, a nearly twofold increase in the compositional percentage of the ash content. The actual ash content may have also increased due to the presence of the additional activating potassium species during the activation. The increase in water content was attributed to the adsorption of atmospheric water vapour, whilst the increase in ash was attributed to the combined effects of  $K^+$  intercalation and the introduction of aluminosilicates due to the corrosion of the combustion boat, as discussed previously.

### 3.2.5. FTIR

FTIR is a useful tool to identify bonds within a given sample. The technique relies upon the molecular vibrations which occur due to the absorption of infrared radiation, the common molecular vibrations are depicted in Fig. 17. Different bonds or functional groups absorb different

**Table 10**  
Proximate analysis of rCF, vCF, ArCF and AvCF.

Sample	C (%)	VOC (%)	Water (%)	Ash (%)
rCF	93.21	2.84	0.00	3.95
vCF	92.80	4.82	0.00	2.38
ArCF	75.30	15.27	1.88	7.55
AvCF	73.66	13.67	4.70	7.97

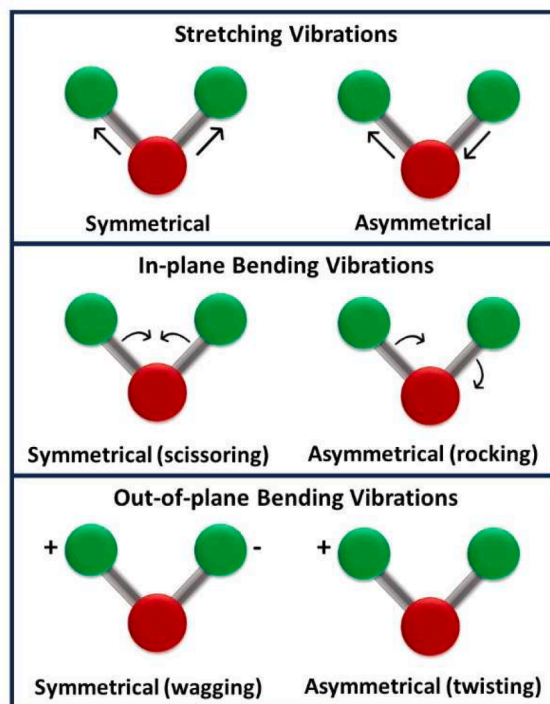


**Fig. 17.** Common molecular vibrations of FTIR, where (–) and (+) signify in-plane and out-of-plane bending, respectively.

frequencies of IR leading to characteristic peaks for each bond. FTIR was applied to analyse rCF and vCF (Fig. 18), ArCF and AvCF (Fig. 19) and ArCF-MB and AvCF-MB (Fig. 20).

Both rCF and vCF show characteristic spectra for PAN-based CFs. The peaks at  $3696$  and  $3650$   $\text{cm}^{-1}$  were attributed to O–H stretching

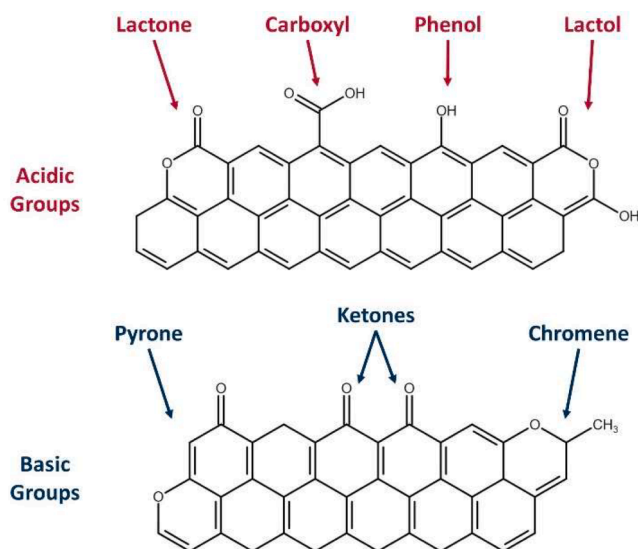


**Fig. 16.** Typical oxygen-containing groups for carbonaceous adsorbents [32].

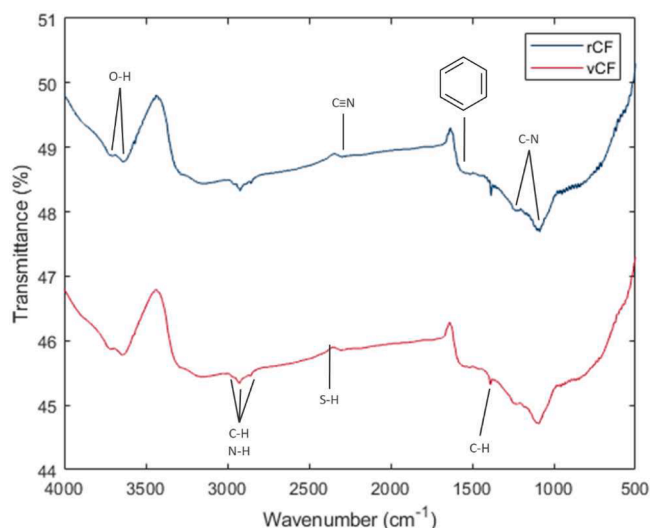


**Fig. 18.** Infrared spectra of rCF (top) and vCF (bottom).

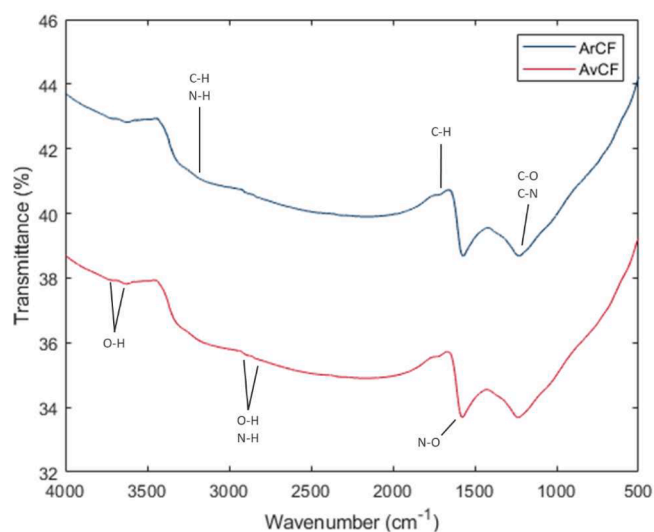


Fig. 19. Infrared spectra of ArCF-Opt (top) and AvCF-Opt (bottom).

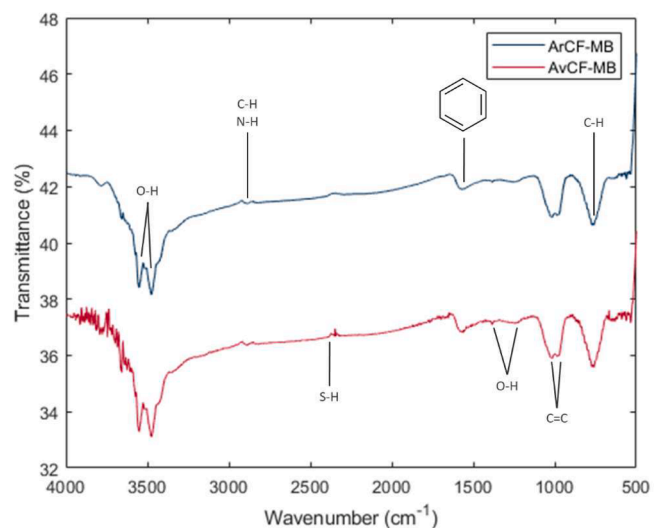


Fig. 20. Infrared spectra of ArCF-Opt (top) and AvCF-Opt (bottom) after adsorption of MB.

vibrations due to the absorption of water by KBr. Whilst the peak at  $3580\text{ cm}^{-1}$  was attributed to N–H stretching vibrations. The peaks present in the range of  $2947\text{--}2844\text{ cm}^{-1}$  are characteristic of C–H bonds, namely CH,  $\text{CH}_2$  and  $\text{CH}_3$ . The presence of nitrile groups ( $\text{C}\equiv\text{N}$ ) within the PAN chain gives rise to the peak at  $2310\text{ cm}^{-1}$ . Whilst the peak at  $1532\text{ cm}^{-1}$  is the stretching vibration, characteristic of aromatic benzene structures. Finally, the peaks between  $1242$  and  $1191$  are characteristic of C–N bending vibrations.

Post-activation, there were some notable changes to the functional groups present. Namely the introduction of peaks at  $1725$ ,  $1351$  and  $1223\text{ cm}^{-1}$ , which were assigned to the introduction of C=O, O–H and C–O groups, respectively. Furthermore, the  $\text{C}\equiv\text{N}$  peak at  $2310\text{ cm}^{-1}$  is absent, indicating the cleavage of bonds during the high temperature activation process.

After adsorption, there are significant changes to the functional groups present within both ACFs, indicating chemisorption processes (Fig. 20). The peaks between  $3664$  and  $3380$  can be assigned to O–H stretching vibrations. The peak at  $2913\text{ cm}^{-1}$  can be attributed to intramolecular bonded C–H and N–H stretching vibrations. Interestingly, there has been a peak introduced at  $2433\text{ cm}^{-1}$ , typical of the S–H stretching vibration of thiol, indicating that the sulphur group within

MB may have formed bonds with an oxygen containing group on the ACF surface. Similarly, to non-activated samples, peaks have been reintroduced at  $1558\text{ cm}^{-1}$ , characteristic of aromatic benzene structures. Whilst the peaks at  $1381$  and  $1236\text{ cm}^{-1}$  can be ascribed to O–H and N–H bending vibrations. The peaks at  $1000\text{--}989\text{ cm}^{-1}$  were attributed to C=C bending vibrations and the peak at  $773\text{ cm}^{-1}$  is the C–H bending vibration of monosubstituted benzene derivatives.

### 3.2.6. Raman

Raman spectroscopy is a powerful tool for analysing carbonaceous adsorbents due to the ability to distinguish between disordered and ordered carbon via the D and G bands which are present in the Raman spectra for both the activated and non-activated samples, at approximately  $1370\text{ cm}^{-1}$  and  $1590\text{ cm}^{-1}$ , respectively (Fig. 21). The D band is an  $A_{1g}$  breathing mode symmetry and is characteristic of disordered  $\text{sp}^3$  hybridised carbon bond stretching [64]. Whereas the G band is of  $E_{2g}$  mode symmetry which is representative of the C–C in-plane stretch of  $\text{sp}^2$  hybridised carbon, within graphitic materials.

Aside from the D and G bands, there are several other peaks present within both samples. The peaks at around  $815$  and  $905\text{ cm}^{-1}$  were attributed to the ring breathing of piperidine and C–N–C stretch of secondary amines, respectively. While the sharp peak at  $2350\text{ cm}^{-1}$  was ascribed to N=C=O pseudo-antisymmetric stretching.

Some additional peaks were introduced for the activated samples, the most interesting being the  $D_4$  band at  $1246\text{ cm}^{-1}$  which is representative of both  $A_{1g}$  symmetry and the presence of ionic impurities, an additional indication of the intercalation of  $\text{K}^+$  into the fibre structure [65]. The peaks at  $1052$ ,  $1114$ ,  $1286$  and  $1552\text{ cm}^{-1}$  were assigned to ortho-disubstituted benzene stretch, N=N stretch,  $\text{NO}_2$  stretch and antisymmetric  $\text{NO}_2$  stretch, respectively.

Interestingly, the peak intensity is significantly increased for the ACFs in comparison to the precursor. An increase in intensity for the D band in particular can be a sign of successful functionalisation, since D band intensity increases linearly with increasing functionalisation up to approximately 6 groups attached per 1000 carbon atoms, providing further evidence with regards to the oxidation of the ACFs [66,67].

## 4. Conclusion

CFRPs are versatile materials which are widely applied in many industries, however large amounts of waste are generated when products reach their EoL. Despite the currently available recycling techniques, rCFs are not typically applied within their former industries due to a reduction in mechanical strength. This study aimed to create an

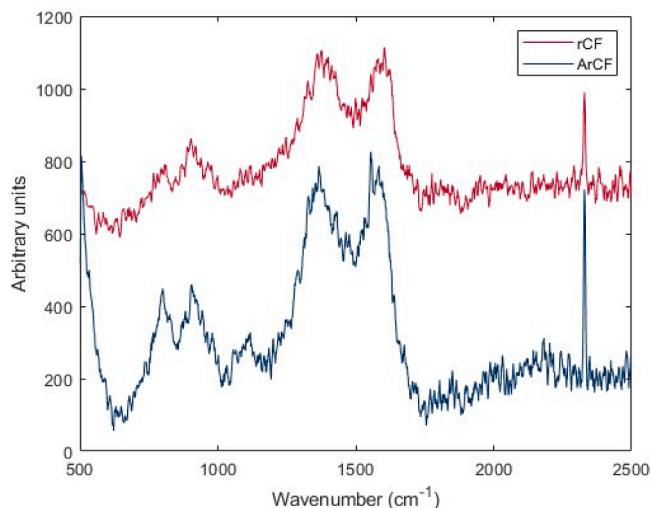


Fig. 21. Raman spectra of rCF (top) and ArCF-Opt (bottom).

alternative EoL pathway for rCFs as adsorbents. Due to the lack of research around the conversion of rCFs to adsorbents, a detailed statistical analysis was undertaken using DoE to optimise the process. rCFs were chemically activated by employing BBD-RSM optimisation techniques to assess the impact of several factors on the responses, i.e. yield and MB adsorption capacity. The optimum conditions were found to be an activation temperature, IR and hold time of 670 °C, 1:10 (CF:KOH) and 0.5 h, respectively. All factors were found to be statistically significant on the response, yield, with activation temperature and IR being most impactful. In contrast, only IR was statistically significant with respect to MB adsorption capacity, with higher levels being most favourable. This was attributed to the enhanced oxidation of the surface at higher IR, which act as active sites for adsorption.

Overall, the optimum ArCF adsorbent had an MB equilibrium adsorption capacity of 454.55 mg/g, above that of its AvCF counterpart (344.83 mg/g). This phenomenon was attributed to the reduction in mechanical strength of the rCF precursor, making the surface more readily etched during the activation procedure, thus increasing the surface area. Furthermore, ArCFs possessed a higher quantity of oxygen-containing groups which act as active sites for adsorption.

Further research is required to determine whether rCFs would be feasible as commercialised aqueous-phase adsorbents. To move forward continuous adsorption systems would need to be investigated to determine the mass transfer zones and breakthrough curves. Furthermore, regeneration efficiency, leaching potential and EoL processes should be investigated. Finally, a further DoE should be undertaken to investigate the optimisation of adsorption processes, to improve the adsorption capacity of the ACFs.

#### CRediT authorship contribution statement

**Jessica H. Taylor:** Writing – original draft, Investigation, Formal analysis, Data curation. **Gera Troisi:** Writing – review & editing, Supervision, Funding acquisition, Conceptualization. **Salman Masoudi Soltani:** Writing – review & editing, Supervision, Resources, Project administration, Investigation, Conceptualization.

#### Declaration of competing interest

The authors declare that they have no known competing financial interests or personal relationships that could have appeared to influence the work reported in this paper.

#### Data availability

All data generated in this paper have been included within the paper, or added to the supplementary material.

#### Acknowledgements

This work has been funded by the UK's Engineering and Physical Sciences Research Council (EPSRC), as part of the UKRI, via the EPSC Doctoral Training Partnership (project reference EP/T518116/1).

Additionally, the authors would like to recognise the Experimental Techniques Centre (ETC) at Brunel University London, UK, and their scientific officers for facilitating access to analytical equipment. For his assistance in coding, the authors would like to thank William George Davies. The authors would also like to thank Gen 2 Carbon for providing the rCF to complete this research.

#### Supplementary materials

Supplementary material associated with this article can be found, in the online version, at [doi:10.1016/j.cej.2024.100591](https://doi.org/10.1016/j.cej.2024.100591).

#### References

- [1] S. Termine, V. Naxaki, D. Semitekolos, A.F. Trompeta, M. Rovere, A. Tagliaferro, et al., Investigation of carbon fibres reclamation by pyrolysis process for their reuse potential, *Polymers (Basel)* 15 (3) (2023) 768, 2023, Vol 15, 768 [Internet]. Feb 2 [cited 2023 May 23] Available from: <https://www.mdpi.com/2073-4360/15/3/768/htm>.
- [2] J. Zhang, V.S. Chevali, H. Wang, C.H. Wang, Current status of carbon fibre and carbon fibre composites recycling, *Compos. B Eng.* 193 (2020) 108053. Jul 15.
- [3] E. Pakdel, S. Kashi, R. Varley, X. Wang, Recent progress in recycling carbon fibre reinforced composites and dry carbon fibre wastes, *Resour. Conserv. Recycl.* 166 (2021) 105340. Mar 1.
- [4] M.A. Nahil, P.T. Williams, Recycling of carbon fibre reinforced polymeric waste for the production of activated carbon fibres, *J. Anal. Appl. Pyrolysis* 91 (1) (2011) 67–75. May 1.
- [5] J.Y. Chen, Activated carbon fibre and textiles [Internet]. Activated Carbon Fiber and Textiles, Elsevier Science & Technology, 2016, pp. 08–25 [cited 2021 Jul 31] Available from: <https://ebookcentral.proquest.com/lib/brunelu/detail.action?docID=4627945>.
- [6] M.F. Hassan, M.A. Sabri, H. Fazal, A. Hafeez, N. Shezad, M. Hussain, Recent trends in activated carbon fibers production from various precursors and applications—a comparative review, *J. Anal. Appl. Pyrolysis* 145 (2020) 104715.
- [7] J. Zhang, G. Lin, U. Vaidya, H. Wang, Past, present and future prospective of global carbon fibre composite developments and applications, *Compos. B Eng.* 250 (2023) 110463. Feb 1.
- [8] S. Karuppanan Gopalraj, T. Käarki, A review on the recycling of waste carbon fibre/glass fibre-reinforced composites: fibre recovery, properties and life-cycle analysis, *SN Appl. Sci.* 2 (3) (2020) 1–21, 2020 2:3 [Internet] Feb 18 [cited 2021 Jul 30] Available from: <https://link.springer.com/article/10.1007/s42452-020-2195-4>.
- [9] A.K. Bledzki, H. Seidlitz, K. Goracy, M. Urbaniak, J.J. Rösch, Recycling of carbon fiber reinforced composite polymers—review—part 1: volume of production, recycling technologies, legislative aspects, *Polymer* 13 (2021) 300 [Internet]. 2021 Jan 19 [cited 2021 Aug 12];13(2):300 Available from: <https://www.mdpi.com/2073-4360/13/2/300/htm>.
- [10] M. Alsaadi, M. Bulut, A. Erklığ, A. Jabbar, Nano-silica inclusion effects on mechanical and dynamic behavior of fiber reinforced carbon/Kevlar with epoxy resin hybrid composites, *Compos. B Eng.* 152 (2018) 169–179. Nov 1.
- [11] K. Dass, S.R. Chauhan, B. Gaur, Study on the effects of nano-aluminum-oxide particulates on mechanical and tribological characteristics of chopped carbon fiber reinforced epoxy composites, *Proc. Inst. Mech. Eng., Part L: J. Mater.: Des. Appl.* 231 (4) (2017) 403–422 [Internet] Jun 1 [cited 2024 Jan 5] Available from: <https://journals.sagepub.com/doi/10.1177/1464420715598798>.
- [12] S.K. Singh, A. Kumar, A. Jain, Effect of nanoparticles dispersion on viscoelastic properties of epoxy-zirconia polymer nanocomposites, in: *IOP Conf. Ser. Mater. Sci. Eng.*, 330, 2018 012001 [Internet] Mar 1 [cited 2024 Jan 5] Available from: <https://iopscience.iop.org/article/10.1088/1757-899X/330/1/012001>.
- [13] S.K. Sushil, A. Kumar, Effect of nanoparticles dispersion on viscoelastic properties of epoxy-zirconia polymer nanocomposites, *IOP Conf. Ser.: Mater. Sci. Eng.* 330 (2018) 012054.
- [14] Suresh J.S., Devi DrMP, Sasidhar Dr.M. Effect on mechanical properties of epoxy hybrid composites modified with titanium oxide (TiO<sub>2</sub>) and silicon carbide (SiC). 2017.
- [15] A. Isa, N. Nosbi, M. Che Ismail, H. Md Akil, W.F.F. Wan Ali, M.F. Omar, A review on recycling of carbon fibres: methods to reinforce and expected fibre composite degradations, *Materials (Basel)* 15 (2022) 4991 [Internet]. 2022 Jul 18 [cited 2024 Jan 5];15(14):4991. Available from: <https://www.mdpi.com/1996-1944/15/14/4991/htm>.
- [16] S. Pimenta, S.T. Pinho, Recycling carbon fibre reinforced polymers for structural applications: technology review and market outlook, *Waste Manag.* 31 (2) (2011) 378–392. Feb 1.
- [17] N. Perry, A. Bernard, F. Laroche, S. Pompidou, Improving design for recycling – application to composites, *CIRP Ann.* 61 (1) (2012) 151–154. Jan 1.
- [18] A. López-Urionabarrenechea, N. Gastelu, E. Acha, B.M. Caballero, A. Orue, A. Jiménez-Suárez, et al., Reclamation of carbon fibers and added-value gases in a pyrolysis-based composites recycling process, *J. Clean. Prod.* 273 (2020) 123173. Nov 10.
- [19] R.J. Tapper, M.L. Longana, A. Norton, K.D. Potter, I. Hamerton, An evaluation of life cycle assessment and its application to the closed-loop recycling of carbon fibre reinforced polymers, *Compos. B Eng.* 184 (2020) 107665. Mar 1.
- [20] S. Verma, B. Balasubramaniam, R.K. Gupta, Recycling, reclamation and re-manufacturing of carbon fibres, *Curr. Opin. Green Sustain. Chem.* 13 (2018) 86–90. Oct 1.
- [21] L. Giorgini, T. Benelli, G. Brancolini, L. Mazzocchetti, Recycling of carbon fibre reinforced composite waste to close their life cycle in a cradle-to-cradle approach, *Curr. Opin. Green Sustain. Chem.* 26 (2020) 100368. Dec 1.
- [22] V.P. McConnell, Launching the carbon fibre recycling industry, *Reinf. Plast.* 54 (2) (2010) 33–37. Mar 1.
- [23] S. Das, Life cycle assessment of carbon fibre-reinforced polymer composites, *Int. J. Life Cycle Assess.* 16 (3) (2011) 268–282 [Internet]. 2011 Feb 22 [cited 2021 Aug 12];16(3) Available from: <https://link.springer.com/article/10.1007/s11367-011-0264-z>.
- [24] R.A. Witik, R. Teuscher, V. Michaud, C. Ludwig, J.A.E. Månson, Carbon fibre reinforced composite waste: an environmental assessment of recycling, energy recovery and landfilling, *Compos. Part A Appl. Sci. Manuf.* 49 (2013) 89–99. Jun 1.
- [25] P. Puri, P. Compston, V. Pantano, Life cycle assessment of Australian automotive door skins, *Int. J. Life Cycle Assess.* 14 (5) (2009) 420–428 [Internet] Jul 21 [cited

- 2024 Jan 5] Available from: <https://link.springer.com/article/10.1007/s11367-009-0103-7>.
- [26] X. Li, R. Bai, J. McKechnie, Environmental and financial performance of mechanical recycling of carbon fibre reinforced polymers and comparison with conventional disposal routes, *J. Clean. Prod.* 127 (2016) 451–460. Jul 20.
- [27] A.K. Bledzki, H. Seidlitz, K. Goracy, M. Urbaniak, J.J. Rösch, Recycling of carbon fiber reinforced composite polymers—review—part I: volume of production, recycling technologies, legislative aspects, *Polymers (Basel)* 13 (2) (2021) 1–13 [Internet] Jan 2 [cited 2023 Oct 23] Available from: <https://pmc/articles/PMC7835776/>.
- [28] T. Lee, C.-H. Ooi, R. Othman, F.-Y. Yeoh, T. Lee, C.-H. Ooi, et al., Activated carbon fiber—the hybrid of carbon fiber and activated carbon, *Rev. Adv. Mater. Sci.* 36 (2014) 118–136.
- [29] H. Marsh, F. Rodríguez-Reinoso, Characterization of activated carbon, *Activated Carbon* (2006) 143–242. Jan 1.
- [30] A. Świątkowski, Industrial carbon adsorbents, *Stud. Surf. Sci. Catal.* 120 (1999) 69–94. Jan 1.
- [31] J.H. Taylor, S Masoudi Soltani, Carbonaceous adsorbents in the removal of aquaculture pollutants: a technical review of methods and mechanisms, *Ecotoxicol. Environ. Saf.* 266 (2023) 115552 [Internet] Nov 1 [cited 2023 Oct 11] Available from: <https://linkinghub.elsevier.com/retrieve/pii/S0147651323010564>.
- [32] Taylor J., Babamohammadi S., Troisi G., Masoudi Soltani S. Chemical activation of recycled carbon fibres for application as porous adsorbents in aqueous media [Internet]. [cited 2022 Nov 17]. Available from: <https://ieeexplore.ieee.org/stamp/stamp.jsp?tp=&arnumber=9928646>.
- [33] D. He, V.K. Soo, F. Stojcevski, W. Lipiński, L.C. Henderson, P. Compston, et al., The effect of sizing and surface oxidation on the surface properties and tensile behaviour of recycled carbon fibre: an end-of-life perspective, *Compos. Part A Appl. Sci. Manuf.* 138 (2020) 106072. Nov 1.
- [34] G. Jiang, S.J. Pickering, G.S. Walker, K.H. Wong, C.D. Rudd, Surface characterisation of carbon fibre recycled using fluidised bed, *Appl. Surf. Sci.* 254 (9) (2008) 2588–2593. Feb 28.
- [35] M. Gorbounov, J. Taylor, B. Petrovic, S Masoudi Soltani, To DoE or not to DoE? A technical review on & roadmap for optimisation of carbonaceous adsorbents and adsorption processes, *S. Afr. J. Chem. Eng.* 41 (2022) 111–128. Jul 1.
- [36] H. Marsh, F. Rodríguez-Reinoso, Activation processes (Chemical), *Activated Carbon* (2006) 322–365. Jan 1.
- [37] S. Rio, C. Faur-Brasquet, Coq L le, P. Courcoux, Cloirec P le, Experimental design methodology for the preparation of carbonaceous sorbents from sewage sludge by chemical activation—application to air and water treatments, *Chemosphere* 58 (4) (2005) 423–437. Jan 1.
- [38] J.A. Maciá-Agulló, B.C. Moore, D. Cazorla-Amorós, A. Linares-Solano, Activation of coal tar pitch carbon fibres: physical activation vs. chemical activation. *Carbon*, Elsevier Ltd, 2004, pp. 1367–1370.
- [39] R. Hoseinzadeh Hesas, A. Arami-Niya, W.M.A. Wan Daud, J.N Sahu, Preparation of granular activated carbon from oil palm shell by microwave-induced chemical activation: optimisation using surface response methodology, *Chem. Eng. Res. Des.* 91 (12) (2013) 2447–2456. Dec 1.
- [40] Jorda M. High surface area carbon nanotubes prepared by chemical activation. 2002.
- [41] M.A. Lillo-Ródenas, D. Cazorla-Amorós, A. Linares-Solano, Understanding chemical reactions between carbons and NaOH and KOH: an insight into the chemical activation mechanism, *Carbon N Y* 41 (2) (2003) 267–275. Feb 1.
- [42] D.S.S. Alkathiri, M.A. Sabri, T.H. Ibrahim, Y.A. ElSayed, F. Jumean, Development of activated carbon fibers for removal of organic contaminants, *Int. J. Environ. Sci. Technol.* 17 (12) (2020) 4841–4852, <https://doi.org/10.1007/s13762-020-02808-8> [Internet] Dec 1 [cited 2021 Mar 3] Available from: .
- [43] Y. Gao, Q. Yue, B. Gao, A. Li, Insight into activated carbon from different kinds of chemical activating agents: a review, *Sci. Total Environ.* 746 (2020) 141094. Dec 1.
- [44] M. Gorbounov, E. Díaz-Vasseur, D. Danaci, S.M. Soltani, Chemical activation of porous carbon extracted from biomass combustion bottom ash for CO<sub>2</sub> adsorption, *Carbon Capture Sci. Technol.* 100151 (2023) [Internet] Oct 14 [cited 2023 Oct 15] Available from: <https://linkinghub.elsevier.com/retrieve/pii/S2772656823000556>.
- [45] P.O. Oladoye, T.O. Ajiboye, E.O. Omotola, O.J. Oyewola, Methylene blue dye: toxicity and potential elimination technology from wastewater, *Results Eng.* 16 (2022) 100678. Dec 1.
- [46] L.S. Maia, A.I.C. da Silva, E.S. Carneiro, F.M. Monticelli, F.R. Pinhati, D. R. Mulinari, Activated carbon from palm fibres used as an adsorbent for methylene blue removal, *J. Polym. Environ.* 29 (4) (2021) 1162–1175 [Internet] Apr 1 [cited 2022 Feb 19] Available from: <https://link.springer.com/article/10.1007/s10924-020-01951-0>.
- [47] Joshi S., Shrestha R.G., Pradhananga R.R., Ariga K., Shrestha L.K. High surface area nanoporous activated carbons materials from areca catechu nut with excellent iodine and methylene blue adsorption. *C* 2022, Vol 8, 2 [Internet]. 2021 Dec 27 [cited 2023 May 26];8(1):2. Available from: <https://www.mdpi.com/2311-5629/8/1/2/htm>.
- [48] I. Khan, K. Saeed, I. Zekker, B. Zhang, A.H. Hendi, A. Ahmad, et al., Review on methylene blue: its properties, uses, toxicity and photodegradation, *Water (Basel)* 14 (2022) 242 [Internet]. 2022 Jan 14 [cited 2023 Oct 22];14(2):242 Available from: <https://www.mdpi.com/2073-4441/14/2/242/htm>.
- [49] J.S. Noh, J.A. Schwarz, Effect of HNO<sub>3</sub> treatment on the surface acidity of activated carbons, *Carbon N Y* 28 (5) (1990) 675–682. Jan 1.
- [50] S.L. Goertzen, K.D. Thériault, A.M. Oickle, A.C. Tarasuk, H.A. Andreas, Standardization of the Boehm titration. Part I. CO<sub>2</sub> expulsion and endpoint determination, *Carbon N Y* 48 (4) (2010) 1252–1261. Apr 1.
- [51] A.M. Oickle, S.L. Goertzen, K.R. Hopper, Y.O. Abdalla, H.A. Andreas, Standardization of the Boehm titration: part II. Method of agitation, effect of filtering and dilute titrant, *Carbon N Y* 48 (12) (2010) 3313–3322. Oct 1.
- [52] C.A. Nunes, M.C. Guerreiro, Estimation of surface area and pore volume of activated carbons by methylene blue and iodine numbers, *Quim. Nova* 34 (3) (2011) 472–476 [Internet] [cited 2023 Jun 13] Available from: <https://www.scielo.br/j/qn/a/VY5JpTFcqRhbzSFZc9xq3J/?lang=en>.
- [53] Shrestha L.K., Thapa M., Shrestha R.G., Maji S., Pradhananga R.R., Ariga K. Rice husk-derived high surface area nanoporous carbon materials with excellent iodine and methylene blue adsorption properties. *C* 2019, Vol 5, Page 10 [Internet]. 2019 Feb 22 [cited 2023 Jun 13];5(1):10. Available from: <https://www.mdpi.com/2311-5629/5/1/10/htm>.
- [54] R. Devesa-Rey, G. Bustos, J.M. Cruz, A.B. Moldes, Optimisation of entrapped activated carbon conditions to remove coloured compounds from winery wastewaters, *Bioresour. Technol.* 102 (11) (2011) 6437–6442. Jun 1.
- [55] M. Gorbounov, B. Petrovic, S. Ozmen, P. Clough, S Masoudi Soltani, Activated carbon derived from biomass combustion bottom ash as solid sorbent for CO<sub>2</sub> adsorption, *Chem. Eng. Res. Des.* 194 (2023) 325–343. Jun 1.
- [56] C. Pelekani, V.L. Snoeyink, Competitive adsorption in natural water: role of activated carbon pore size, *Water Res.* 33 (5) (1999) 1209–1219. Apr 1.
- [57] V.M. Gun'ko, Competitive adsorption, *Theor. Exp. Chem.* 43 (3) (2007) 139–183, 43:3 [Internet]. 2007 May [cited 2022 Jan 25] Available from: <https://link.springer.com/article/10.1007/s11237-007-0020-4>.
- [58] M.C. Silva, L. Spessato, T.L. Silva, G.K.P. Lopes, H.G. Zanella, J.T.C. Yokoyama, et al., H<sub>3</sub>PO<sub>4</sub>-activated carbon fibers of high surface area from banana tree pseudo-stem fibers: adsorption studies of methylene blue dye in batch and fixed bed systems, *J. Mol. Liq.* 324 (2021) 114771. Feb 15.
- [59] Q.X. Liu, Y.R. Zhou, M. Wang, Q. Zhang, T. Ji, T.Y. Chen, et al., Adsorption of methylene blue from aqueous solution onto viscose-based activated carbon fiber felts: kinetics and equilibrium studies, *Adsorp. Sci. Technol.* 37 (3–4) (2019) 312–332 [Internet] May 1 [cited 2023 Aug 11] Available from: <https://journals.sagepub.com/doi/full/10.1177/0263617419827437>.
- [60] B. Liu, C. Du, J.J. Chen, J.Y. Zhai, Y. Wang, H.L. Li, Preparation of well-developed mesoporous activated carbon fibers from plant pulp fibers and its adsorption of methylene blue from solution, *Chem. Phys. Lett.* 771 (2021) 138535. May 16.
- [61] A.H. Jawad, N.N. Mohd Firdaus Hum, A.S. Abdulhameed, M.A. Mohd Ishak, Mesoporous activated carbon from grass waste via H<sub>3</sub>PO<sub>4</sub>-activation for methylene blue dye removal: modelling, optimisation, and mechanism study, *Int. J. Environ. Anal. Chem.* (2020) [Internet] [cited 2023 Jan 26] Available from: <https://www.tandfonline.com/doi/abs/10.1080/03067319.2020.1807529>.
- [62] C. Cheng, J. Zhang, Y. Mu, J. Gao, Y. Feng, H. Liu, et al., Preparation and evaluation of activated carbon with different polycondensed phosphorus oxyacids (H<sub>3</sub>PO<sub>4</sub>, H<sub>4</sub>P<sub>2</sub>O<sub>7</sub>, H<sub>6</sub>P<sub>4</sub>O<sub>13</sub> and C<sub>6</sub>H<sub>18</sub>O<sub>24</sub>P<sub>6</sub>) activation employing mushroom roots as precursor, *J. Anal. Appl. Pyrolysis* 108 (2014) 41–46 [Internet] [cited 2023 Aug 11] Available from: [https://www.researchgate.net/publication/262937843\\_P\\_reparation\\_and\\_evaluation\\_of\\_activated\\_carbon\\_with\\_different\\_polycondensed\\_phosphorus\\_oxyacids\\_H3PO4\\_H4P2O7\\_H6P4O13\\_and\\_C6H18O24P6\\_activation\\_employing\\_mushroom\\_roots\\_as\\_precursor](https://www.researchgate.net/publication/262937843_P_reparation_and_evaluation_of_activated_carbon_with_different_polycondensed_phosphorus_oxyacids_H3PO4_H4P2O7_H6P4O13_and_C6H18O24P6_activation_employing_mushroom_roots_as_precursor).
- [63] S. Katz, A. Pevzner, V. Shepelev, S. Marx, H. Rotter, T. Amitay-Rosen, et al., Activated carbon aging processes characterization by Raman spectroscopy, *MRS Adv.* 7 (12) (2022) 245–248 [Internet] Apr 1 [cited 2023 Oct 22] Available from: <https://link.springer.com/article/10.1557/43580-021-00189-9>.
- [64] A. Sadezky, H. Muckenhuber, H. Grothe, R. Niessner, U. Pöschl, Raman microspectroscopy of soot and related carbonaceous materials: spectral analysis and structural information, *Carbon N Y* 43 (8) (2005) 1731–1742. Jul 1.
- [65] R. Graupner, Raman spectroscopy of covalently functionalized single-wall carbon nanotubes, *J. Raman Spectrosc.* 38 (6) (2007) 673–683 [Internet] Jun 1 [cited 2023 Oct 22] Available from: <https://onlinelibrary.wiley.com/doi/full/10.1002/jrs.1694>.
- [66] M.S. Strano, C.A. Dyke, M.L. Usrey, P.W. Barone, M.J. Allen, H. Shan, et al., Electronic structure control of single-walled carbon nanotube functionalization, *Science* 301 (5639) (2003) 1519–1522 [Internet] Sep 12 [cited 2023 Oct 22] Available from: <https://pubmed.ncbi.nlm.nih.gov/12970561/>.